Computer-Aided Design 78 (2016) 126–136

Contents lists available at ScienceDirect

Computer-Aided Design

journal homepage: www.elsevier.com/locate/cad

Boundary-aware hodge decompositions for piecewise constant vector fields☆

Konstantin Poelke *, Konrad Polthier

Freie Universität Berlin, Germany

ARTICLE INFO

Keywords:
Hodge decomposition
Piecewise constant vector fields
Harmonic fields
Simplicial surface with boundary

ABSTRACT

We provide a theoretical framework for discrete Hodge-type decomposition theorems of piecewise constant vector fields on simplicial surfaces with boundary that is structurally consistent with decomposition results for differential forms on smooth manifolds with boundary. In particular, we obtain a discrete Hodge–Morrey–Friedrichs decomposition with subspaces of discrete harmonic Neumann fields $\mathcal{H}_{h,N}$ and Dirichlet fields $\mathcal{H}_{h,D}$, which are representatives of absolute and relative cohomology and therefore directly linked to the underlying topology of the surface. In addition, we discretize a recent result that provides a further refinement of the spaces $\mathcal{H}_{h,N}$ and $\mathcal{H}_{h,D}$, and answer the question in which case one can hope for a complete orthogonal decomposition involving both spaces at the same time.

As applications, we present a simple strategy based on iterated L^2-projections to compute refined Hodge-type decompositions of vector fields on surfaces according to our results, which give a more detailed insight than previous decompositions. As a proof of concept, we explicitly compute harmonic basis fields for the various significant subspaces and provide exemplary decompositions for two synthetic vector fields.

1. Introduction

Hodge-type decomposition theorems form a class of central results in the study of vector fields and, more generally, differential forms on manifolds, with far-reaching applications ranging from the detection of topologically nontrivial regions and vector field analysis to the prediction of existence of solutions for PDEs. If the underlying manifold is closed, these decompositions reduce to the phrase "exact" plus "coexact" plus "harmonic", with the space of all harmonic fields being isomorphic to a certain cohomology space—a remarkable result known as de Rham's theorem. However, in the presence of a boundary, these decompositions become much more subtle. For instance, without any further assumptions, exact and coexact fields are no longer orthogonal to each other. In fact, they span the whole space of all fields, so there is no harmonic complement left, and one has to impose certain boundary conditions to recover the relation to the topology of the underlying geometry. Accordingly, a consistent discretization of Hodge-type theorems in the presence of a boundary is of great importance with regard to computational applications.

Piecewise constant vector fields (PCVFs) are widely used in discretization methods for differential geometric quantities on simplicial surfaces. Being defined by one tangent vector per triangle, they provide an intuitive representation for velocity and force fields in fluid dynamics or computational electromagnetics, principal curvature direction fields in shape analysis or frame fields in modeling, parametrization, and remeshing tasks in geometry processing, just to name a few examples. Moreover, they arise naturally as surface gradients of linear Lagrange elements frequently used in FEM systems, including e.g. discretizations of curvature flows or the computation of minimal surfaces. However, since a PCVF is totally discontinuous and uncoupled, the operators involved in the smooth theory do not exist for PCVFs, not even in a weak sense, and it is a priori not clear how to discretize the differentiable calculus in order to preserve the structural results of the smooth Hodge decomposition.

In this article we present a complete description of the space $\mathcal{X}_h$ of PCVFs on simplicial surfaces with boundary in terms of various Hodge-type decomposition results which are structurally consistent with their smooth counterparts in terms of topological relevance, dimension and exactness. These results give rise to a full understanding of $\mathcal{X}_h$, incorporate the sources of topological

☆ This paper has been recommended for acceptance by Scott Schaefer and Charlie C.L. Wang.

* Corresponding author.
E-mail address: konstantin.poelke@fu-berlin.de (K. Poelke).

http://dx.doi.org/10.1016/j.cad.2016.05.004
0010-4485/

nontriviality that arise on surfaces with boundary – cohomology induced by boundary loops and cohomology induced by interior handles – and therefore allow for a precise characterization of PCVFs. Surprisingly, it turns out that the surface mesh has to satisfy a certain criterion for some of the discrete analogues to hold, and this criterion is not of a topological, but a combinatorial nature, i.e. depends on the triangulation, and we will give several examples below. In addition, we present a straightforward and easy to implement strategy for the computation of representative harmonic basis fields for topologically significant subspaces, and propose a refined Hodge-type decomposition method using iterated L^2-projections – two applications that are of fundamental importance in geometry processing and vector field analysis on surfaces.

Related work

Hodge-type decompositions on smooth manifolds are a classical topic, see e.g. [1]. The refinement of Dirichlet and Neumann fields into subspaces representing inner and boundary cohomology is apparently due to Hermann Gluck and Dennis DeTurck, but to the best of our knowledge first published in [2,3].

Discrete Hodge decompositions are still an active field of research, see [4] for a survey. Of the recent developments, see [5] for a decomposition in the spectral domain, Bhatia [6] for decompositions with natural boundary conditions on unbounded domains, or Ribeiro [7] for a decomposition of vector field ensembles to highlight correlations.

Piecewise constant vector fields on surfaces are present in geometric discretization schemes on surfaces at least since the work by Polthier and Preuss [8] for singularity detection and vector field decomposition, and a further investigation for closed surfaces based on this approach has been given in [9]. Previous to that, they have been used in discontinuous Galerkin methods for numerical simulations, although in this field their usage mostly restricts to problems on flat domains embedded in $\mathbb{R}^2$, which do not exhibit any interior nontrivial cohomology.

Since then there has been published an extensive amount of articles that deal with discretization schemes for vector fields and differential forms on simplicial geometries in various flavors:

Hirani [10] proposes a framework called *discrete exterior calculus (DEC)* that interprets discrete differential forms as cochains on a simplicial complex. A subset of all PCVFs (the rotation-free fields) can be regarded as closed 1-forms in this setting, but the notion of coexactness and the corresponding ansatz space differ from our approach. Hirani [11] extends this work by computing harmonic fields representing cohomology generators.

The work by Arnold [12] gives a precise numerical treatment of complexes of finite element spaces constituting a discrete de Rham complex on planar domains, focusing on stability issues for mixed problems that are deduced from a careful choice of ansatz spaces. A special case is the complex of lowest order Whitney interpolants, isomorphic to the cochain complex in DEC. Convergence estimates generalizing their results to approximating meshes are given in [13].

The paradigm of preserving the structural properties of the smooth world in the discretization is also prevalent to mimetic methods, see [14,15], in particular with respect to discretization of complexes. The idea is to discretize the operators in such a way that essential structural relations such as Green's formula are enforced to hold.

Applications of PCVFs include e.g. frame field generation and deformation of meshes with gradients of harmonic functions as in [16], field generation via quasi-harmonic potentials as in [17], or quadrilateral meshing algorithms as in [18,19].

2. Smooth decompositions

In this section we briefly summarize several smooth Hodge-type decompositions on manifolds with boundaries. For details, we refer to Schwarz [1], Abraham [20] and the survey article by Bhatia [4].

2.1. Hodge decomposition on manifolds with boundary

Starting with the physically motivated Helmholtz decomposition of a vector field inside a three-dimensional domain into a solenoidal and a conservative component in the 19th century, there is a long history of generalizations and refinements of similar decomposition statements. The *Hodge decomposition* extends the domain to arbitrary smooth manifolds M and generalizes the objects to be decomposed to differential forms, including the classical Helmholtz decomposition as the special case of 1-forms on open sets in $\mathbb{R}^3$. For closed n-dimensional smooth manifolds it states that the space of k-forms Ω^k can be L^2-orthogonally decomposed as

$$\Omega^k = \mathrm{d}\Omega^{k-1} \oplus \delta\Omega^{k+1} \oplus \mathcal{H}^k$$

where $\mathcal{H}^k$ denotes the space of *harmonic k-forms*, being simultaneously in the kernel of the exterior derivative d as well as the coderivative δ. Furthermore, the de Rham isomorphism identifies the space $\mathcal{H}^k$ as a space of representatives for the kth singular cohomology group $H^k(M)$. Here and in the following, all cohomology is understood as cohomology with real coefficients, and later on we implicitly refer to simplicial cohomology on the discretized surface, and $\oplus$ always denotes an L^2-orthogonal direct sum.

In the presence of a boundary ∂M, the spaces of exact forms $\mathrm{d}\Omega^{k-1}$ and coexact forms $\delta\Omega^{k+1}$ are no longer L^2-orthogonal to each other. To circumvent this problem one usually poses *Dirichlet boundary conditions* (the tangential part $\mathrm{tang}(\omega)$ of a differential form has to vanish along the boundary ∂M) on the space Ω^{k-1} and *Neumann boundary conditions* (the normal part $\omega|_{\partial M} - \mathrm{tang}(\omega)$ has to vanish along ∂M) on Ω^{k+1} to obtain a decomposition

$$\Omega^k = \mathrm{d}\Omega_D^{k-1} \oplus \delta\Omega_N^{k+1} \oplus \mathcal{H}^k.$$

However, in this splitting the space of harmonic forms $\mathcal{H}^k$ is now infinite-dimensional and has no topological significance anymore. Friedrichs has observed [21] that $\mathcal{H}^k$ can be further split into subspaces of *Dirichlet* and *Neumann fields*, isomorphic to relative and absolute cohomology. This leads to the *Hodge–Morrey–Friedrichs (HMF) decomposition*

$$\Omega^k = \mathrm{d}\Omega_D^{k-1} \oplus \delta\Omega_N^{k+1} \oplus \mathcal{H} \cap \mathrm{d}\Omega^{k-1} \oplus \mathcal{H}_N^k \tag{1}$$

$$= \mathrm{d}\Omega_D^{k-1} \oplus \delta\Omega_N^{k+1} \oplus \mathcal{H} \cap \delta\Omega^{k+1} \oplus \mathcal{H}_D^k \tag{2}$$

with $\mathcal{H}_N^k \cong H^k(M)$ and $\mathcal{H}_D^k \cong H^k(M, \partial M)$, where the latter denotes the kth relative cohomology space of M. Furthermore, it is

$$\mathcal{H}_N^k \cap \mathcal{H}_D^k = \{0\}, \tag{3}$$

a highly nontrivial result which can be considered an analogue of an identity-type theorem known from complex analysis (see e.g. [22]).

2.2. Inner and boundary cohomology

The decompositions in Eqs. (1) and (2) raise the question whether there is a single orthogonal decomposition involving both the spaces $\mathcal{H}_D^k$ and $\mathcal{H}_N^k$ at the same time, but this is in general not possible. Recent results [3,2] identify the obstacle as the subspace of inner cohomology representatives within $\mathcal{H}_D^k$ and $\mathcal{H}_N^k$ which

cause the orthogonality to fail. Therein, the following spaces are defined:

$$\mathcal{H}^k_{N,\mathrm{co}} := \mathcal{H}^k_N \cap \delta\Omega^{k+1}(M) \tag{4}$$

$$\mathcal{H}^k_{N,\partial\mathrm{ex}} := \{\omega \in \mathcal{H}^k_N : \iota^*\omega \in \mathrm{d}\Omega^{k-1}(\partial M)\} \tag{5}$$

$$\mathcal{H}^k_{D,\mathrm{ex}} := \mathcal{H}^k_D \cap \mathrm{d}\Omega^{k-1}(M) \tag{6}$$

$$\mathcal{H}^k_{D,\partial\mathrm{co}} := \star\mathcal{H}^{n-k}_{N,\partial\mathrm{ex}} \tag{7}$$

which are coined *coexact* and *boundary-exact* Neumann fields, and *exact* and *boundary-coexact* Dirichlet fields, respectively, the last one being defined as the image of $\mathcal{H}^{n-k}_{N,\partial\mathrm{ex}}$ under the Hodge star isomorphism, and ι^* denotes the pull-back along the inclusion $\iota : \partial M \hookrightarrow M$. As proved in [2], these spaces give a refined decomposition:

$$\mathcal{H}^k_N = \mathcal{H}^k_{N,\mathrm{co}} \oplus \mathcal{H}^k_{N,\partial\mathrm{ex}} \tag{8}$$

$$\mathcal{H}^k_D = \mathcal{H}^k_{D,\mathrm{ex}} \oplus \mathcal{H}^k_{D,\partial\mathrm{co}}. \tag{9}$$

In the following we are interested in the case that M is a compact, oriented surface with boundary and $k = 1$. By the classification theorem for surfaces, every such surface is homeomorphic to a surface $\Sigma_{g,m}$ which is a g-fold torus with m disjoint holes cut in. Then by Poincaré-Lefschetz duality it is $h^1 := \dim H^1(M) = \dim H^1(M, \partial M) = 2g + m - 1$, and combining the previous decompositions we obtain

$$\Omega^1 = \mathrm{d}\mathcal{C}^\infty_0 \oplus \delta\Omega^2_N \oplus \mathrm{d}\mathcal{C}^\infty \cap \delta\Omega^2 \oplus (\mathcal{H}^1_N + \mathcal{H}^1_D)$$

where $\mathcal{C}^\infty$ denotes the space of smooth functions on M and $\mathcal{C}^\infty_0$ is its subspace of all functions that vanish on ∂M. If $g = 0$, the sum $\mathcal{H}^1_N + \mathcal{H}^1_D$ is not only direct, but also L^2-orthogonal, see Lemma 3.10 for the same argument in the discrete case.

3. Discrete Hodge-type decompositions

We will now transfer the smooth results from Section 2 to the setting of piecewise constant vector fields on triangulated surfaces and obtain a structurally consistent discretization of several Hodge-type decompositions on surfaces with boundary. A translation of differential forms into the classical language of vector analysis can be found in [20] or Schwarz [1].

Throughout, we assume that M_h is an oriented, compact topological surface with (not necessarily connected) boundary ∂M_h, embedded in $\mathbb{R}^3$, triangulated by a finite, affine simplicial complex structure, so that ∂M_h is triangulated by a subcomplex. For brevity, we refer to M_h as a *simplicial surface*. We denote by n_V the number of vertices of the triangulation, n_{bV} the number of *boundary vertices*, i.e. the vertices of the subcomplex triangulating ∂M_h, and $n_{iV} := n_V - n_{bV}$ the number of *inner vertices*, and similarly for the number of edges n_E and triangles n_T.

3.1. Function spaces on simplicial surfaces

A *piecewise constant vector field (PCVF)* on M_h is an element $X \in L^2(M_h, \mathbb{R}^3)$ such that $X|_T$ is represented by a constant tangent vector field in the tangent plane over each triangle T, and we denote the space of all PCVFs by $\mathcal{X}_h$. Hence one can identify an element $X \in \mathcal{X}_h$ with a family $(X_T)_{T\in M_h}$ indexed by the triangles of M_h, where X_T is a vector in the plane through the origin parallel to T. The L^2-product on $\mathcal{X}_h$ then reduces to a sum of weighted Euclidean scalar products as

$$\langle X, Y\rangle_{L^2} = \sum_{T\in M_h} \langle X_T, Y_T\rangle \cdot \mathrm{area}(T).$$

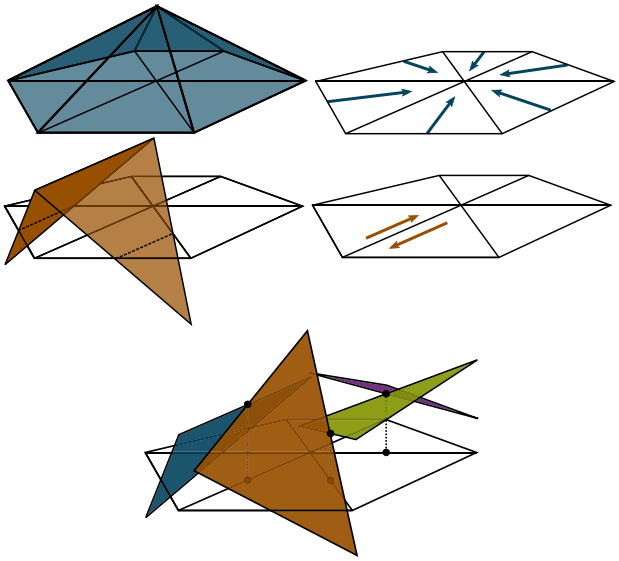

Fig. 1. First row: Lagrange basis function associated to the middle vertex and its gradient field. Second row: Crouzeix–Raviart basis function associated to an edge and its cogradient field. Third row: A general Crouzeix–Raviart function is only continuous at edge midpoints. (For interpretation of the references to color in this figure legend, the reader is referred to the web version of this article.)

For the discretization of potential and copotential functions we use the following, well-known ansatz spaces: the space of *linear Lagrange* elements is defined as

$$\mathcal{L} := \left\{ \varphi : \begin{array}{l} \varphi|_T \text{ linear on each triangle } T \text{ and} \\ \varphi \text{ globally continuous} \end{array} \right\}.$$

The space of *Crouzeix–Raviart* elements or *edge-based* elements is defined as

$$\mathcal{F} := \left\{ \psi : \begin{array}{l} \psi|_T \text{ linear on each triangle } T \text{ and} \\ \psi \text{ continuous at edge midpoints} \end{array} \right\}.$$

Functions in $\mathcal{L}$ are uniquely determined by their function values at vertices of the triangulation, whereas functions in $\mathcal{F}$ are uniquely determined by their function values at edge midpoints, and a canonical basis is given by all functions that evaluate to 1 at a particular vertex (or edge midpoint) and 0 at all other vertices (or edge midpoints, respectively), see Fig. 1. Hence, the number of degrees of freedom, i.e. the dimension of these spaces, is the number of vertices n_V for $\mathcal{L}$ and the number of edges n_E for $\mathcal{F}$. We define subspaces $\mathcal{L}_0 \subset \mathcal{L}$ and $\mathcal{F}_0 \subset \mathcal{F}$ as those spaces consisting of all functions whose degrees of freedom associated with simplices on the boundary are set to zero:

$$\mathcal{L}_0 := \{\varphi \in \mathcal{L} : \varphi(v_b) = 0 \text{ at all bnd. vertices } v_b\}$$

$$\mathcal{F}_0 := \{\psi \in \mathcal{F} : \psi(m_{e_b}) = 0 \text{ at all bnd. edge midpoints } m_{e_b}\}.$$

The discrete surface gradient ∇, defined piecewise over each triangle as the smooth surface gradient, maps both function spaces $\mathcal{L}$ and $\mathcal{F}$ to subspaces of $\mathcal{X}_h$.

The orientation on M_h induces a discrete Hodge star isomorphism $J : \mathcal{X}_h \to \mathcal{X}_h$, defined piecewise over every triangle. If $(N_T)_{T\in M_h}$ denotes the (discrete) unit normal field of M_h, then J acts on an element $X \in \mathcal{X}_h$ as

$$(JX)_T := N_T \times X_T$$

where $\times$ is the Euclidean cross product in $\mathbb{R}^3$. Thus it can be interpreted as a counter-clockwise rotation by $\pi/2$ in the tangent

plane at each triangle. We define the following (co-)gradient spaces:

$$\nabla\mathcal{L}_{(0)} := \{\nabla\varphi : \varphi \in \mathcal{L}_{(0)}\}$$
$$J\nabla\mathcal{F}_{(0)} := \{J\nabla\psi : \psi \in \mathcal{F}_{(0)}\},$$

possibly with boundary conditions imposed on the function spaces.

Lemma 3.1. *An element $X \in \mathcal{X}_h$ is tangentially continuous across inner edges if and only if $X \in (J\nabla\mathcal{F}_0)^\perp$, the L^2-orthogonal complement of $J\nabla\mathcal{F}_0$ within $\mathcal{X}_h$. In particular, $(J\nabla\mathcal{F}_0)^\perp$ and $(J\nabla\mathcal{F})^\perp$ are isomorphic to the space of closed simplicial 1-cochains $\mathcal{Z}^1(M_h)$ and closed relative simplicial 1-cochains $\mathcal{Z}^1_0(M_h)$ on M_h, respectively.*

Proof. The first statement is a direct computation and follows from the local nature of the cogradient $J\nabla\psi_e$ of a basis function $\psi_e \in \mathcal{F}$ associated to an edge e, see Fig. 1. The identification of $J\nabla\mathcal{F}_0^\perp$ with the space of closed 1-cochains works as follows: assign an arbitrary orientation to all edges $e \in M_h$ and define a simplicial 1-cochain $w_X \in C^1(M_h)$ by $w_X(e) := \langle X_{T'}, e\rangle$, where T' is a triangle adjacent to e. Since $X \in (J\nabla\mathcal{F}_0)^\perp$ is tangentially continuous, it does not matter which triangle T' we choose for inner edges, so this assignment is well-defined. It is easy to check that the resulting cochain is closed and that, conversely, one can reconstruct the vector field X by knowing its tangential projections onto the edges only (if these values come from a closed cochain, this reconstruction step is not overdetermined). This gives an isomorphism $\Phi : (J\nabla\mathcal{F}_0)^\perp \to \mathcal{Z}^1(M_h), X \mapsto w_X$. If $\psi_{e_b} \in \mathcal{F}$ is a function associated to a boundary edge e_b with adjacent triangle T_b, then $\langle X, J\nabla\psi_{e_b}\rangle_{L^2} = 0$ forces X_{T_b} to be perpendicular to e_b, and therefore $w_X(e_b) = 0$. Thus, Φ restricts to an isomorphism $\Phi_0 : (J\nabla\mathcal{F})^\perp \to \mathcal{Z}^1_0(M_h)$ onto the space of closed relative 1-cochains. □

In particular, the gradient field $\nabla\varphi$ of a linear Lagrange function $\varphi \in \mathcal{L}$ is tangentially continuous, since φ is globally continuous and the tangential projection of its gradient field onto an edge e is just the slope of the restricted function $\varphi|_e$, so that $\nabla\varphi \in J\nabla\mathcal{F}_0^\perp$. Furthermore, for each $\varphi \in \mathcal{L}_0$, its gradient $\nabla\varphi$ is perpendicular to the boundary and therefore has vanishing tangential projection on the boundary.

These two observations show that $\nabla\mathcal{L} \subseteq J\nabla\mathcal{F}_0^\perp$ and $\nabla\mathcal{L}_0 \subseteq J\nabla\mathcal{F}^\perp$. Define the spaces $\mathcal{H}_h$, $\mathcal{H}_{h,N}$ and $\mathcal{H}_{h,D}$ as the L^2-orthogonal complement of the orthogonal sums $\nabla\mathcal{L}_0 \oplus J\nabla\mathcal{F}_0$, $\nabla\mathcal{L} \oplus J\nabla\mathcal{F}_0$ and $\nabla\mathcal{L}_0 \oplus J\nabla\mathcal{F}$ within $\mathcal{X}_h$, respectively. We refer to them as *discrete harmonic fields*, *discrete Neumann fields* and *discrete Dirichlet fields*.

Note that whereas discrete Dirichlet fields are truly perpendicular to the boundary edges, discrete Neumann fields are only "almost parallel" along the boundary, see Fig. 2. Being orthogonal to $J\nabla\mathcal{F}$ enforces the vector field to be strictly perpendicular to all boundary edges e_b, since each $J\nabla\psi_{e_b}$ is supported over a single triangle only (the one adjacent to e_b). In contrast, being orthogonal to a gradient $\nabla\varphi_{v_b}$ of a Lagrange function associated to a boundary vertex v_b is a condition over all triangles in the star of v_b, and thus a more global condition.

3.2. Discrete Hodge-type decompositions

From the previous discussion we immediately obtain two decompositions we refer to as *fundamental decompositions* in the following.

Theorem 3.2 (*Fundamental Decomposition*)**.** *The space $\mathcal{X}_h$ has the following L^2-orthogonal decompositions*

$$\mathcal{X}_h = \nabla\mathcal{L} \oplus J\nabla\mathcal{F}_0 \oplus \mathcal{H}_{h,N} \tag{10}$$
$$= \nabla\mathcal{L}_0 \oplus J\nabla\mathcal{F} \oplus \mathcal{H}_{h,D} \tag{11}$$

and it is $\dim\mathcal{H}_{h,N} = \dim\mathcal{H}_{h,D} = h^1$, the first Betti number of M_h. In particular, bases for $\mathcal{H}_{h,N}$ and $\mathcal{H}_{h,D}$ constitute a concrete choice of cohomology generators of $H^1(M_h)$ and $H^1(M_h, \partial M_h)$, respectively.

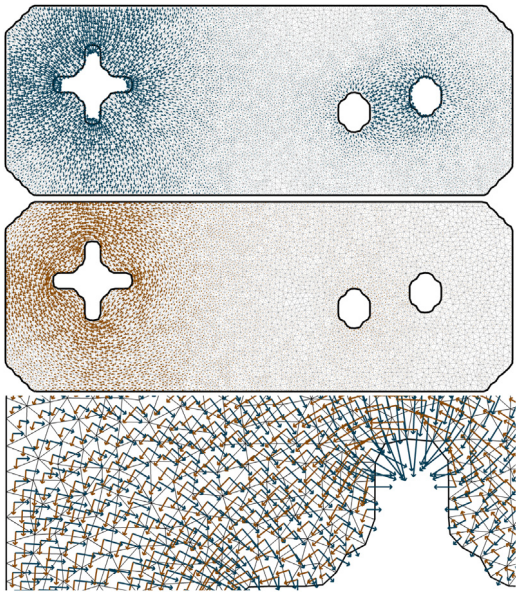

Fig. 2. A discrete Dirichlet field (top) and Neumann field (middle) on a flat geometry of type $\Sigma_{0,4}$, each being one out of three basis fields for $\mathcal{H}_{h,D}$ and $\mathcal{H}_{h,N}$. The bottom image shows a close-up of both fields in a vicinity of boundary components. The Dirichlet field (blue) along the boundary is orthogonal to each boundary edge, whereas the Neumann field is only almost tangential. Both fields are L^2-orthogonal to each other, since all Dirichlet fields are exact (and correspondingly, all Neumann fields are coexact), and here, they appear almost orthogonal even on individual triangles over wide regions of the geometry. (For interpretation of the references to color in this figure legend, the reader is referred to the web version of this article.)

Proof. The orthogonality follows from Section 3.1. For the dimensions, one can perform a direct computation using the identities for the Euler characteristic $\chi(M_h) = n_V - n_E + n_T = 1 - h^1$. However, the following argument is more insightful since it directly identifies the spaces $\mathcal{H}_{h,N}$ and $\mathcal{H}_{h,D}$ as representatives for the absolute and relative first cohomology: the classical Whitney interpolation map (see [23] or Arnold [12]) provides an isomorphism $W : C^0(M_h) \to \mathcal{L}$ from simplicial 0-cochains to linear Lagrange elements, and restricts to an isomorphism $W_0 : C^0_0(M_h) \to \mathcal{L}_0$ on relative 0-cochains. One checks that the following diagrams commute, the vertical arrows being isomorphisms, and d_S being the derivative on the level of simplicial cochains (the adjoint to the simplicial boundary operator):

$$\begin{array}{ccc} \mathcal{L} & \xrightarrow{\nabla} & J\nabla\mathcal{F}_0^\perp \\ {\scriptstyle W}\uparrow & & \downarrow{\scriptstyle \Phi} \\ C^0(M_h) & \xrightarrow{\mathrm{d}_S} & \mathcal{Z}^1(M_h) \end{array} \qquad \begin{array}{ccc} \mathcal{L}_0 & \xrightarrow{\nabla} & J\nabla\mathcal{F}^\perp \\ {\scriptstyle W_0}\uparrow & & \downarrow{\scriptstyle \Phi_0} \\ C^0_0(M_h) & \xrightarrow{\mathrm{d}_S} & \mathcal{Z}^1_0(M_h) \end{array}$$

It follows that $\mathcal{H}_{h,N} \cong H^1(M_h)$ and $\mathcal{H}_{h,D} \cong H^1(M_h, \partial M_h)$, and by Lefschetz–Poincaré duality it is $H^1(M_h) \cong H^1(M_h, \partial M_h)$. □

As a corollary we obtain discrete analogues of the HMF-decompositions in Eqs. (1) and (2):

Corollary 3.3 (*Discrete HMF-Decomposition*)**.**

$$\mathcal{X}_h = \nabla\mathcal{L}_0 \oplus J\nabla\mathcal{F}_0 \oplus \mathcal{H}_h \cap \nabla\mathcal{L} \oplus \mathcal{H}_{h,N}$$
$$= \nabla\mathcal{L}_0 \oplus J\nabla\mathcal{F}_0 \oplus \mathcal{H}_h \cap J\nabla\mathcal{F} \oplus \mathcal{H}_{h,D}.$$

If M_h is a closed surface of genus g, both decompositions reduce to

$$\mathcal{X}_h = \nabla\mathcal{L} \oplus J\nabla\mathcal{F} \oplus \mathcal{H}_h$$

with $\dim\mathcal{H}_h = 2g$, as stated in [9].

3.3. When is $\mathcal{H}_{h,N} \cap \mathcal{H}_{h,D} = \{0\}$?

As in the smooth case, a central question towards a consistent discretization is whether the discrete version $\mathcal{H}_{h,N} \cap \mathcal{H}_{h,D} = \{0\}$ of Eq. (3) holds true, too. With respect to the fundamental decompositions in Theorem 3.2, this question is equivalent to the equality

$$\mathcal{X}_h = \nabla\mathcal{L} + J\nabla\mathcal{F}. \tag{12}$$

But in contrast to the smooth theory, this is not always the case, as a simple calculation shows: computing dimensions, we have $\dim \mathcal{X}_h = 2n_T$, $\dim \nabla\mathcal{L} = n_V - 1$ and $\dim J\nabla\mathcal{F} = n_E - 1$. So even if we assume a direct sum (i.e. $\nabla\mathcal{L} \cap J\nabla\mathcal{F} = \{0\}$), then by subtracting the relation $3n_T - 2n_E + n_{bE} = 0$ we obtain

$$\begin{aligned}
&\dim \mathcal{X}_h - \dim(\nabla\mathcal{L} + J\nabla\mathcal{F}) \\
&= 2n_T - (n_V - 1) - (n_E - 1) \\
&= 2n_T - n_V - n_E + 2 - (3n_T - 2n_E + n_{bE}) \\
&= -\chi(M_h) + 2 - n_{bE} = h^1 + 1 - n_{bE}.
\end{aligned}$$

Therefore, even in the most optimistic case $\nabla\mathcal{L} \cap J\nabla\mathcal{F} = \{0\}$ this difference will be positive whenever $h^1 + 1 > n_{bE}$, i.e. if the discretization of the boundary is too low in comparison with the topological complexity, and the difference is even larger if we do not assume trivial intersection.

The situation is even more involved: even if $n_{bE} \geq h^1 + 1$, it still might be the case that Eq. (12) does not hold. The reason for this failure are cycles (i.e. closed paths) in M_h that are homologous to boundary cycles (or more generally sums of boundary cycles) and have a substantially smaller number of edges, preventing a cohomology basis to be uniquely associated with prescribed values at edges. However, in general it is not clear how to state precise conditions that are easy to verify for a given surface M_h, as it also depends on the distribution of boundary components across the surface. Most geometries that arise in practice and possess reasonable triangulations satisfy Eq. (12). Particular care must be taken, though, if M_h has a very high genus in comparison to the number of boundary components (i.e. if $g \gg m$), if the grid discretization around the boundary holes is particularly coarse, or if M_h can be roughly divided into a region capturing the boundaries and a region of high genus, both connected only by a very coarse discretization, for instance. See Fig. 3 for some prototypical examples.

For the rest of this article we assume that Eq. (12) *is satisfied on* M_h. We then obtain

Corollary 3.4. *It is* $\mathcal{H}_{h,N} \cap \mathcal{H}_{h,D} = \{0\}$, *as in the smooth case.*

Proof. Clearly, the intersection $\mathcal{H}_{h,N} \cap \mathcal{H}_{h,D}$ is orthogonal to both $\nabla\mathcal{L}$ and $J\nabla\mathcal{F}$, but since Eq. (12) is satisfied it follows $\nabla\mathcal{L}^\perp \cap J\nabla\mathcal{F}^\perp = (\nabla\mathcal{L} + J\nabla\mathcal{F})^\perp = \{0\}$. □

This gives a refined result of the discrete HMF-decompositions in Corollary 3.3, in which both the spaces $\mathcal{H}_{h,N}$ and $\mathcal{H}_{h,D}$ appear simultaneously:

Corollary 3.5 (*Central Harmonic Decomposition*)**.** $\mathcal{X}_h$ *has the splitting*

$$\mathcal{X}_h = \nabla\mathcal{L}_0 \oplus J\nabla\mathcal{F}_0 \oplus \nabla\mathcal{L} \cap J\nabla\mathcal{F} \oplus (\mathcal{H}_{h,N} + \mathcal{H}_{h,D}),$$

and the central harmonic space $\nabla\mathcal{L} \cap J\nabla\mathcal{F}$ *has dimension* $n_{bE} - h^1 - 1$, *tending to infinity under refinement of the boundary.*

The sum $\mathcal{H}_{h,N} + \mathcal{H}_{h,D}$ is in general not L^2-orthogonal, but merely direct. Therefore, the natural questions that arise are whether it is actually possible that $\mathcal{H}_{h,N}$ and $\mathcal{H}_{h,D}$ are orthogonal to each other, and if so, under what conditions does this happen?

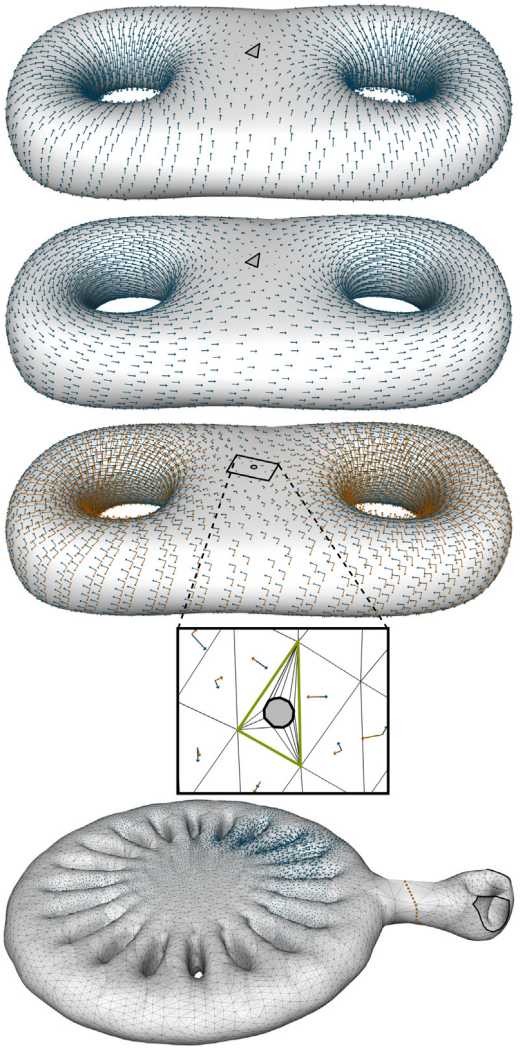

Fig. 3. First three images: pretzel surface with a single triangle cut out, so $n_{bE} = 3 < 5 = h^1 + 1$, and Eq. (12) does not hold. The shown fields form a basis for the nontrivial intersection space $\mathcal{H}_{h,N} \cap \mathcal{H}_{h,D}$ (first two images). But even if n_{bE} is large enough, such fields can still exist (third image). The reason are edge cycles in M_h which are homologous to the boundary and constitute a coarse *virtual boundary* (green line) as shown in the close-up of the boundary hole. Last image: on the low-discretized tunnel connecting the high-genus region of a surface of type $\Sigma_{21,2}$ with the boundary region there is an edge cycle homologous not to a single boundary component, but to the sum of both boundary cycles, constituting a boundary cycle with just 8 edges. These are too few to associate all homology generators for the high-genus part independently to boundary edges, where they are forced to be zero. As a consequence, a large number of fields in $\mathcal{H}_{h,N} \cap \mathcal{H}_{h,D}$ exist on this geometry. (For interpretation of the references to color in this figure legend, the reader is referred to the web version of this article.)

Remark 3.6. The obstruction mentioned in this section is a surprising and remarkable fact not present in the smooth counterpart: whereas the dimensions of $\mathcal{H}_{h,N}$ and $\mathcal{H}_{h,D}$ are of a purely topological nature, the question whether they have a trivial intersection now relies on a combinatorial quantity of the grid, and is therefore not invariant under topology-preserving retriangulations. It should be kept in mind for sanity checks of the discretization strategy.

3.4. Boundary and inner cohomology

Next, we consider discrete analogues of the coexact and boundary-exact Neumann fields and the corresponding distinction

of Dirichlet fields. In analogy with Eq. (4) we define

$$\mathcal{H}_{h,N,\mathrm{co}} := \mathcal{H}_{h,N} \cap J\nabla\mathcal{F}$$
$$\mathcal{H}_{h,N,\partial\mathrm{ex}} := \mathcal{H}_{h,N,\mathrm{co}}^{\perp} \cap \mathcal{H}_{h,N}$$
$$\mathcal{H}_{h,D,\mathrm{ex}} := \mathcal{H}_{h,D} \cap \nabla\mathcal{L}$$
$$\mathcal{H}_{h,D,\partial\mathrm{co}} := \mathcal{H}_{h,D,\mathrm{ex}}^{\perp} \cap \mathcal{H}_{h,D}$$

and refer to them as *discrete coexact Neumann fields* and so on. We have the refined splittings

$$\mathcal{H}_{h,N} = \mathcal{H}_{h,N,\mathrm{co}} \oplus \mathcal{H}_{h,N,\partial\mathrm{ex}}$$
$$\mathcal{H}_{h,D} = \mathcal{H}_{h,D,\mathrm{ex}} \oplus \mathcal{H}_{h,D,\partial\mathrm{co}},$$

and directly from the definition and the discrete HMF-decompositions Corollary 3.3 we obtain

Corollary 3.7. *It is* $\mathcal{H}_{h,N,\mathrm{co}} \perp \mathcal{H}_{h,D}$ *and* $\mathcal{H}_{h,D,\mathrm{ex}} \perp \mathcal{H}_{h,N}$.

As in the smooth case, these spaces are of topological significance and permit to distinguish between Dirichlet fields that capture homology information that is induced by the boundary (and therefore related to the number m), and homology that arises from homology generators associated to handles of M_h.

Lemma 3.8. *Let* M_h *be homeomorphic to* $\Sigma_{g,m}$. *Then it is* $\dim \mathcal{H}_{h,D,\mathrm{ex}} = m - 1$.

Proof. Consider the following part from the long exact cohomology sequence

$$\cdots \to H^0(\partial M_h) \xrightarrow{\delta^*} H^1(M_h, \partial M_h) \xrightarrow{\pi^*} H^1(M_h) \to \cdots . \tag{13}$$

By Corollary 3.3, a basis for $\mathcal{H}_{h,D}$ represents a basis for the relative cohomology space $H^1(M_h, \partial M_h)$. The map π^* induces a map $\mathrm{pr}_N : \mathcal{H}_{h,D} \to \mathcal{H}_{h,N}$ by making the following diagram commutative:

$$\begin{array}{ccc} \mathcal{H}_{h,D} & \overset{\mathrm{pr}_N}{\dashrightarrow} & \mathcal{H}_{h,N} \\ \downarrow R_D & & \downarrow R_N \\ H^1(M_h, \partial M_h) & \xrightarrow{\pi^*} & H^1(M_h) \end{array}$$

The vertical maps are isomorphisms and can be considered as discrete analogues of the de Rham isomorphism: R_D maps an element $X \in \mathcal{H}_{h,D}$ to the equivalence class of the cocycle $\Phi_0(X)$. Its inverse maps a cohomology class $[w]$ to the element $X := \Phi_0^{-1}(w)$, decomposes X according to Eq. (11) as $X = \nabla\varphi_0 + X_D$ with $X_D \in \mathcal{H}_{h,D}$, and drops the gradient part $\nabla\varphi_0$. Note that it does not depend on the representative w of $[w]$, and is therefore well-defined. A similar description applies to R_N, using Eq. (10). The induced map pr_N then takes an element $X_D \in \mathcal{H}_{h,D}$, decomposes it according to Eq. (10) as $X_D = \nabla\varphi + X_N$ with $X_N \in \mathcal{H}_{h,N}$, and drops the exact component $\nabla\varphi$. It follows that $\mathrm{pr}_N(X_D) = 0$ if and only if $X_D = \nabla\varphi$ for some $\varphi \in \mathcal{L}$, i.e. if X_D is a gradient field, so $X_D \in \mathcal{H}_{h,D,\mathrm{ex}}$. By commutativity of the above diagram it is $\dim \mathcal{H}_{h,D,\mathrm{ex}} = \dim\ker(\pi^*)$, and computing the dimensions in the cohomology sequence gives $\dim\ker(\pi^*) = m - 1$. □

Indeed, since by exactness of the sequence Eq. (13) it is $\ker(\pi^*) = \mathrm{im}(\delta^*)$, we can think of elements in $\mathcal{H}_{h,D,\mathrm{ex}}$ as Dirichlet fields representing nontrivial cohomology information that comes from the boundary components, so we say that $\mathcal{H}_{h,D,\mathrm{ex}}$ represents *boundary cohomology*. Since $h^1 = 2g + m - 1$ this gives $\dim \mathcal{H}_{h,D,\partial\mathrm{co}} = 2g$ for the complementary space, and accordingly we think of these elements as representatives for the *interior cohomology* which is generated by the handles of M_h.

A similar result holds for the splitting of the discrete Neumann space $\mathcal{H}_{h,N}$ due to its symmetric definition: setting $A := \mathcal{H}_h \cap J\nabla\mathcal{F}$ and $B := \mathcal{H}_h \cap \nabla\mathcal{L}$, it is $\mathcal{H}_{h,D,\mathrm{ex}} = B \cap A^{\perp_{\mathcal{H}_h}}$ and $\mathcal{H}_{h,N,\mathrm{co}} = A \cap B^{\perp_{\mathcal{H}_h}}$, where $\perp_{\mathcal{H}_h}$ denotes the L^2-orthogonal complement within the space $\mathcal{H}_h$. Now, from the equations

$$\dim A^{\perp_{\mathcal{H}_h}} = \dim \mathcal{H}_{h,D} = h^1 = \dim \mathcal{H}_{h,N} = \dim B^{\perp_{\mathcal{H}_h}}$$
$$\dim(A \cap B^{\perp_{\mathcal{H}_h}}) = \dim \mathcal{H}_h - \dim(A \cap B^{\perp_{\mathcal{H}_h}})^{\perp_{\mathcal{H}_h}}$$
$$\dim(A \cap B^{\perp_{\mathcal{H}_h}})^{\perp_{\mathcal{H}_h}} = \dim(A^{\perp_{\mathcal{H}_h}} + B)$$
$$\dim(A^{\perp_{\mathcal{H}_h}} + B) = \dim A^{\perp_{\mathcal{H}_h}} + \dim B - \dim(A^{\perp_{\mathcal{H}_h}} \cap B)$$

we obtain, in accordance with the duality in Eq. (8):

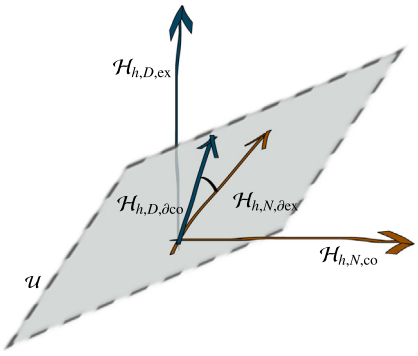

Fig. 4. Schematic, low-dimensional alignment of the spaces $\mathcal{H}_{h,D}$ and $\mathcal{H}_{h,N}$. Both subspaces $\mathcal{H}_{h,N,\partial\mathrm{ex}}$ and $\mathcal{H}_{h,D,\partial\mathrm{co}}$ lie in a common subspace $\mathcal{U}$ (dashed plane) that is orthogonal to both $\mathcal{H}_{h,D,\mathrm{ex}}$ and $\mathcal{H}_{h,N,\mathrm{co}}$. However, $\mathcal{H}_{h,N,\partial\mathrm{ex}}$ and $\mathcal{H}_{h,D,\partial\mathrm{co}}$ are not orthogonal to each other in $\mathcal{U}$, destroying the orthogonality of $\mathcal{H}_{h,D}$ and $\mathcal{H}_{h,N}$. (For interpretation of the references to color in this figure legend, the reader is referred to the web version of this article.)

Lemma 3.9. *It is*

$$\dim \mathcal{H}_{h,D,\mathrm{ex}} = \dim \mathcal{H}_{h,N,\mathrm{co}} = m - 1 \tag{14}$$
$$\dim \mathcal{H}_{h,D,\partial\mathrm{co}} = \mathcal{H}_{h,N,\partial\mathrm{ex}} = 2g, \tag{15}$$

with the spaces in Eq. (14) constituting representatives for the cohomology information generated by the boundary components, whereas the spaces in Eq. (15) represent the interior cohomology information induced by handles. Furthermore, $\mathrm{pr}_N : \mathcal{H}_{h,D,\partial\mathrm{co}} \to \mathcal{H}_{h,N,\partial\mathrm{ex}}$ *is an isomorphism.*

Proof. We only need to show the last statement. Let $X_D \in \mathcal{H}_{h,D,\partial\mathrm{co}}$. Write

$$X_D = \nabla\varphi + Y_{\partial\mathrm{ex}} + J\nabla\psi \in \nabla\mathcal{L} \oplus \mathcal{H}_{h,N,\partial\mathrm{ex}} \oplus \mathcal{H}_{h,N,\mathrm{co}}.$$

Then from $\langle X_D, J\nabla\psi\rangle_{L^2} = 0$ it follows $J\nabla\psi = 0$, so $\mathrm{pr}_N(X_D) = Y_{\partial\mathrm{ex}} \in \mathcal{H}_{h,N,\partial\mathrm{ex}}$. Due to dimension reasons, it must be $\mathrm{im}(\mathrm{pr}_N) = \mathcal{H}_{h,N,\partial\mathrm{ex}}$. □

This gives a result for surfaces that are homeomorphic to $\Sigma_{0,m}$, and covers in particular the case of domains in $\mathbb{R}^2$ with boundary holes, which do not possess any interior homology:

Lemma 3.10. *Let* M_h *be homeomorphic to* $\Sigma_{0,m}$, *then*

$$\mathcal{X}_h = \nabla\mathcal{L}_0 \oplus J\nabla\mathcal{F}_0 \oplus \nabla\mathcal{L} \cap J\nabla\mathcal{F} \oplus \mathcal{H}_{h,N} \oplus \mathcal{H}_{h,D}.$$

Proof. In this case it is $h^1 = m - 1$ and a computation of the dimensions of the spaces in the cohomology sequence Eq. (13) shows that π^* must be the zero map, hence pr_N maps every $X_D \in \mathcal{H}_{h,D}$ to zero, which is equivalent to saying that $\mathcal{H}_{h,D} = \mathcal{H}_{h,D,\mathrm{ex}}$. Corollaries 3.7 and 3.5 give the result. □

In the presence of inner cohomology these spaces are not orthogonal due to the nontrivial subspaces $\mathcal{H}_{h,D,\partial\mathrm{co}}$ and $\mathcal{H}_{h,N,\partial\mathrm{ex}}$, whose elements are concentrated along the inner cohomology generators both spaces share, as shown in Fig. 5. A schematic visualization of this situation is given in Fig. 4. Still, we obtain refined versions of the HMF-decompositions in Corollary 3.3:

Theorem 3.11. *The discrete HMF-decompositions have the following refinements into boundary- and inner-cohomology-representing subspaces:*

$$\mathcal{X}_h = \nabla\mathcal{L}_0 \oplus J\nabla\mathcal{F}_0 \oplus \mathcal{H}_h \cap \nabla\mathcal{L} \oplus \mathcal{H}_{h,N,\mathrm{co}} \oplus \mathcal{H}_{h,N,\partial\mathrm{ex}} \tag{16}$$

$$= \nabla\mathcal{L}_0 \oplus J\nabla\mathcal{F}_0 \oplus \mathcal{H}_h \cap J\nabla\mathcal{F} \oplus \mathcal{H}_{h,D,\mathrm{ex}} \oplus \mathcal{H}_{h,D,\partial\mathrm{co}}. \tag{17}$$

In the situation of Lemma 3.10, both decompositions can be combined to a single orthogonal decomposition involving all the refined spaces at the same time.

4. Applications

We now present two applications for the structural decomposition results derived above. All computations are carried out with the help of the *FEniCS* library [24,25], which we mainly use for the high-level assembly methods of the involved system matrices, and the *JavaView* library [26] for visualization. For the iterative eigensolvers we use the *ARPACK* package as wrapped by the Python library *SciPy*, which provides an efficient implementation of an Arnoldi iteration [27].

Given a simplicial surface mesh M_h, piecewise constant vector fields can be intrinsically represented by picking two directed edges $e_{T,1}, e_{T,2}$ of each triangle T, and writing X_T as a linear combination $\sum_i a_{T,i} e_{T,i}$. Assuming that no triangle is degenerated, these edges form a basis for the tangent plane to T when interpreted as vectors in $\mathbb{R}^3$. In practice, however, such vector fields are usually defined in Euclidean coordinates of the ambient space, where each vector X_T is specified as a vector in $\mathbb{R}^3$, and we will stick to this formulation. It has the advantage that their definition is intuitive and computations can often be easily performed as operations on $\mathbb{R}^3$ without any need of coordinate transformations. On the other hand, the property of being tangential to M_h usually needs to be enforced explicitly and added as a linear constraint.

To compute the surface gradient $\nabla\varphi$ of a function $\mathcal{L}$ or the cogradient $J\nabla\psi$ for $\psi \in \mathcal{F}$, there are again two options: by representing these vector fields as intrinsic quantities expressed in terms of the weighted and rotated edges of M_h, see e.g. [28], or via pull-back to a reference element as done e.g. in [29].

4.1. Computing representatives for cohomology bases

As a first application we compute bases for the topologically significant spaces $\mathcal{H}_{h,D}$ and $\mathcal{H}_{h,N}$ and their refined subspaces of (co-)exact and boundary-(co-)exact Dirichlet and Neumann fields, respectively. From a combinatorial point of view the computation of (co-)homology generators is a central topic in computational topology, see e.g. [30,31] or Busaryev [32], just to name a few exemplary articles. For geometric and physical applications, though, it is often desirable to work with a basis that is formed by harmonic fields as they constitute an even flow, being divergence-free and rotation-free at the same time. Since the property of being divergence-free depends on the Riemannian metric, such a basis cannot be constructed by purely combinatorial methods any more, and one has to incorporate an orthogonalization procedure, see [11]. In the following we therefore compute orthogonal complements of gradient and cogradient spaces directly to obtain bases for $\mathcal{H}_{h,D}$ and $\mathcal{H}_{h,N}$. Theorem 3.2 guarantees that these bases will indeed generate the respective cohomology groups.

Recall that discrete Dirichlet fields are defined as the orthogonal complement of the sum $\nabla\mathcal{L}_0 \oplus J\nabla\mathcal{F}$. Let $\mathcal{B}_{\mathcal{L}} := \{\varphi_i\}$ be the nodal basis of $\mathcal{L}$, and $\mathcal{B}_{\mathcal{L}_0} := \{\varphi_{0,i}\} \subset \mathcal{B}_{\mathcal{L}}$ be the subset of basis functions whose degrees of freedom correspond to the inner vertices. Similarly, let $\mathcal{B}_{\mathcal{F}} := \{\psi_i\}$ and $\mathcal{B}_{\mathcal{F}_0}$ be the edge-midpoint bases for $\mathcal{F}$ and $\mathcal{F}_0$, respectively, the latter containing all basis functions associated to inner edges. To represent elements in $\mathcal{X}_h$, we follow the second approach mentioned above and interpret each vector field $X \in \mathcal{X}_T$ as a family of vectors in $\mathbb{R}^3$, indexed by the triangles T. Without the requirement for tangency, a basis is then given by the family $\{E_{T,1}, E_{T,2}, E_{T,3}\}_{T\in M_h}$ with the canonical basis vectors $E_{T,i} = (\delta_{1,i}, \delta_{2,i}, \delta_{3,i}) \in \mathbb{R}^3$, where $\delta_{i,j}$ denotes the Kronecker delta. For simplicity we re-enumerate these vectors and set $\mathcal{B}_{\mathcal{R}} := \{E_j\}$ for $j = 1, \ldots, 3n_T$, and $\mathcal{R} := \mathbb{R}^{3n_T}$. We define the following matrices:

$$L_{\nabla\mathcal{L}_0,\mathcal{R}} := \left(\langle\nabla\varphi_{0,i}, E_j\rangle_{L^2}\right)_{\substack{i=1,\ldots,n_{iV}\\ j=1,\ldots,3n_T}}$$

$$L_{J\nabla\mathcal{F},\mathcal{R}} := \left(\langle J\nabla\psi_i, E_j\rangle_{L^2}\right)_{\substack{i=1,\ldots,n_E-1\\ j=1,\ldots,3n_T}}$$

$$L_{\mathcal{N},\mathcal{R}} := \left(\langle N_i, E_j\rangle_{L^2}\right)_{\substack{i=1,\ldots,n_T\\ j=1,\ldots,3n_T}},$$

where N_i is the (constant) normal field of triangle T_i. For an element $X = \sum_i X_i E_i$ in the linear span of $\mathcal{B}_{\mathcal{R}}$ it is $L_{\nabla\mathcal{L}_0,\mathcal{R}} \cdot X = 0$ and $L_{J\nabla\mathcal{F},\mathcal{R}} \cdot X = 0$ if and only if X is L^2-orthogonal to all gradient fields of inner Lagrange elements and all cogradient fields of Crouzeix–Raviart elements on M_h, respectively. Furthermore, $L_{\mathcal{N},\mathcal{R}} \cdot X = 0$ if and only if X is a tangential vector field to M_h. Stacking these matrices into a single matrix

$$L_{\mathcal{H}_{h,D}} := \begin{pmatrix} L_{\nabla\mathcal{L}_0,\mathcal{R}} \\ L_{J\nabla\mathcal{F},\mathcal{R}} \\ L_{\mathcal{N},\mathcal{R}} \end{pmatrix} \tag{18}$$

of dimension $(n_{iV} + n_E - 1 + n_T) \times 3n_T$, it is

$$\mathcal{H}_{h,D} = \ker(L_{\mathcal{H}_{h,D}}),$$

so finding a basis of $\mathcal{H}_{h,D}$ is equivalent to finding a basis for $\ker(L_{\mathcal{H}_{h,D}})$. Note that only $n_E - 1$ basis functions of $\mathcal{F}$ are needed, as the constant functions form the kernel of $J\nabla$. Of course, if M_h is embedded in $\mathbb{R}^2$, there is no need to enforce tangency and one rather computes directly in coordinates of $\mathbb{R}^2$, so the system reduces to a $((n_{iV} + n_E - 1) \times 2n_T)$-matrix.

The matrix $L_{\mathcal{H}_{h,D}}$ is a fairly large and non-square, but sparse matrix, whose kernel is of size h^1 and therefore usually very small in comparison to the matrix size. To solve for its kernel, we apply an ad-hoc strategy and compute almost-zero eigenvectors for the $(3n_T \times 3n_T)$-square matrix

$$M_{\mathcal{H}_{h,D}} := L^t_{\mathcal{H}_{h,D}} \cdot L_{\mathcal{H}_{h,D}}.$$

They can be efficiently computed with iterative solvers that provide an option for a partial computation of the eigenspectrum. Therefore we only need to compute the h^1-many eigenvectors corresponding to the lowest eigenvalues. Here, there are two options: if we know the dimension of the first cohomology in advance, we can provide this number to the solver and obtain h^1-many solutions. On the contrary, if we do not know this number, it seems still possible to deduce the correct number, for we always observed a clear gap in the order of the found eigenvalues when solving for the smallest ones in our experiments, see Fig. 6. Hence, one can stop the iteration once this gap exceeds a certain threshold, often of magnitude 10^5 or higher. The resulting eigenvectors for the h^1 smallest eigenvalues then constitute a basis for the space $\mathcal{H}_{h,D}$. Technically, solving for smallest eigenvalues usually yields very slow convergence for iterative solvers, though, so we use a shift-inversion to transform this eigenproblem into an equivalent problem, which is then solved for the largest eigenvalues, see [27] for details.

The very same strategy can be applied to obtain a basis for $\mathcal{H}_{h,N}$, using the matrices $L_{\nabla\mathcal{L},\mathcal{R}}$ and $L_{J\nabla\mathcal{F}_0,\mathcal{R}}$ instead of $L_{\nabla\mathcal{L}_0,\mathcal{R}}$ and $L_{J\nabla\mathcal{F},\mathcal{R}}$ in the stacked system Eq. (18).

To compute a basis for $\mathcal{H}_{h,D,\mathrm{ex}}$, we proceed in a similar fashion. However, since we are seeking gradient fields, a solution X can be written as $X = \nabla\varphi_X := \sum_i X_i \nabla\varphi_i$. This reduces drastically the

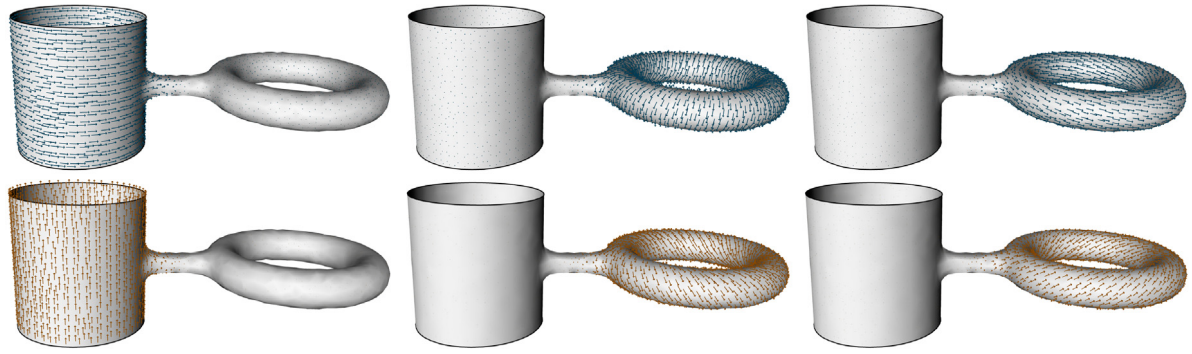

Fig. 5. Basis fields for $\mathcal{H}_{h,N}$ (top row) and $\mathcal{H}_{h,D}$ (bottom row) on a torus with a cylinder attached, which is topologically $\Sigma_{1,2}$. The obstruction for the non-orthogonality of $\mathcal{H}_{h,D}$ and $\mathcal{H}_{h,N}$ lies in the presence of nontrivial inner cohomology generators which are shared by both spaces. Although the representing fields are almost orthogonal on the cylindrical region, they concentrate in the same fashion along the longitudinal and latitudinal cycles that reflect homology generated by the torus, and are clearly not orthogonal to each other any more. All fields are non-zero everywhere, even if the small values are not visible in this graphic. (For interpretation of the references to color in this figure legend, the reader is referred to the web version of this article.)

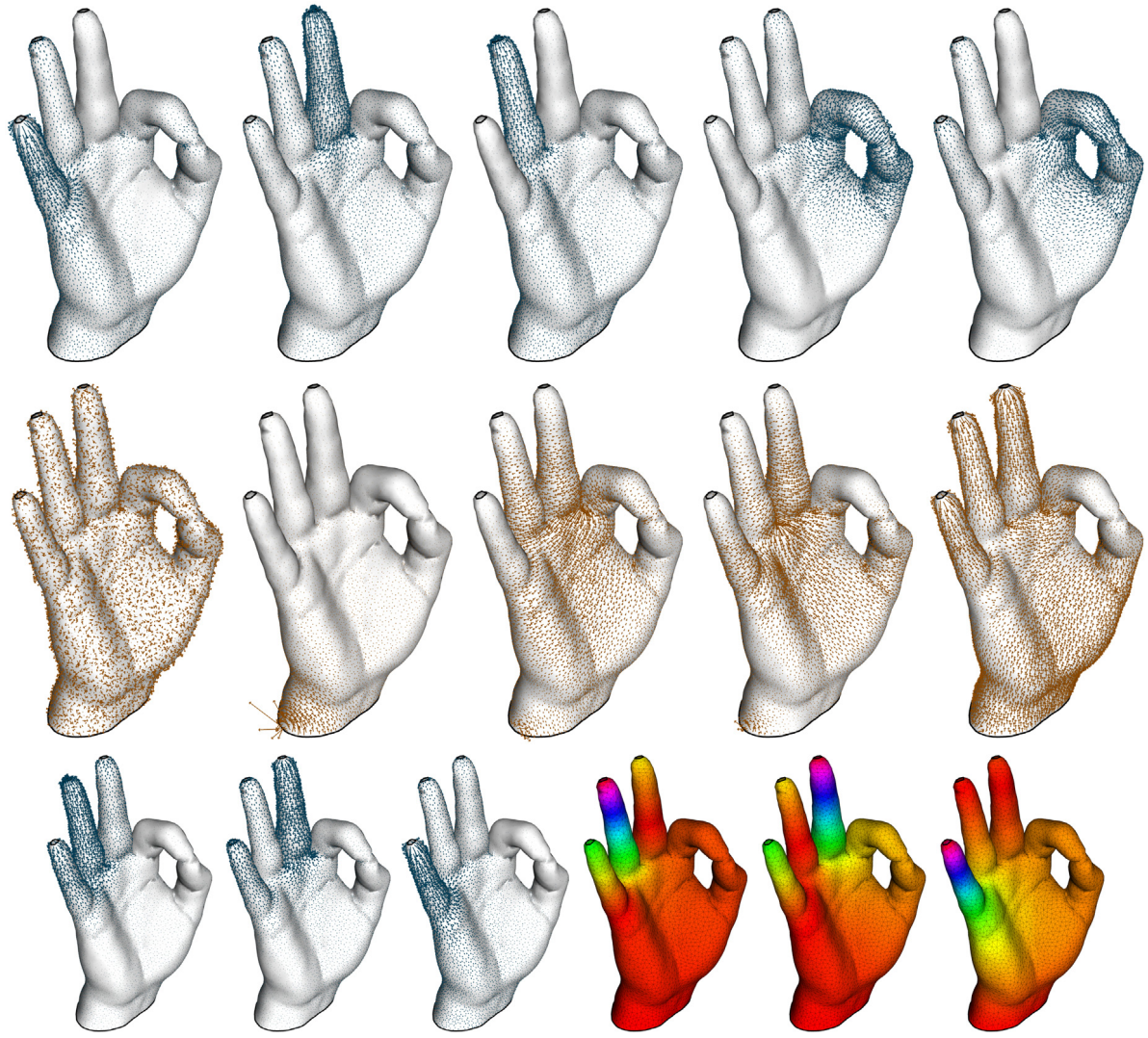

Fig. 6. First row: Basis for $\mathcal{H}_{h,D}$ on the Laurent's hand model with three holes cut into the finger tips and a fourth hole at the wrist, all of them eigenvectors to almost-zero eigenvalues of machine precision order 10^{-16}. Second row: eigenvectors for the next five smallest eigenvalues. This eigenvalues are of orders 10^{-7} to 10^{-3}, so there is a clearly visible gap of magnitude in the eigenspectrum. Whereas some of these eigenvectors are obviously nonsense (first two images), others can give surprisingly well-structured vector fields, depending on the eigenvalue solver. Although the results in the first row already suggest a splitting into $\mathcal{H}_{h,D,\mathrm{ex}}$ (first three images) and $\mathcal{H}_{h,D,\partial\mathrm{co}}$ (last two), this is merely coincidence and cannot be relied on, as it depends on the subspace construction of the iterative solver. In contrast, the third row shows a true basis for $\mathcal{H}_{h,D,\mathrm{ex}}$ and their corresponding harmonic potential functions, being constant on each boundary component. (For interpretation of the references to color in this figure legend, the reader is referred to the web version of this article.)

system size for two reasons: first, no tangency conditions need to be imposed and second, such gradient fields are automatically orthogonal to $J\nabla\mathcal{F}_0$. In effect, there are just two conditions that need to be satisfied for $\nabla\varphi_X$, namely that $\nabla\varphi_X$ is orthogonal to $\nabla\mathcal{L}_0$, and that it is orthogonal to all boundary-cogradients $J\nabla\psi_{b,j}$, where $\psi_{b,j} \in \mathcal{F}$ is a basis function associated to a boundary edge. A solution is then the gradient field of a discrete harmonic function φ_X which is constant on each boundary component, see Fig. 6. We set up the matrices

$$L_{\nabla\mathcal{L}_0,\nabla\mathcal{L}} := \left(\langle\nabla\varphi_{0,i}, \nabla\varphi_j\rangle_{L^2}\right)_{\substack{i=1,\dots,n_{iV}\\ j=1,\dots,n_V}}$$

$$L_{J\nabla\mathcal{F}_b,\nabla\mathcal{L}} := \left(\langle J\nabla\psi_{b,i}, \nabla\varphi_j\rangle_{L^2}\right)_{\substack{i=1,\dots,n_{bE}\\ j=1,\dots,n_V}}$$

and stack them to a matrix

$$L_{\mathcal{H}_{h,D,\mathrm{ex}}} := \begin{pmatrix} L_{\nabla\mathcal{L}_0,\nabla\mathcal{L}} \\ L_{J\nabla\mathcal{F}_b,\nabla\mathcal{L}} \\ (1,0,\dots,0)\end{pmatrix},$$

where the last row is added to exclude constant functions. Solving for the $(m-1)$ eigenvectors to the zero eigenvalues of the $(n_V \times n_V)$-square matrix

$$M_{\mathcal{H}_{h,D,\mathrm{ex}}} := L^t_{\mathcal{H}_{h,D,\mathrm{ex}}} \cdot L_{\mathcal{H}_{h,D,\mathrm{ex}}},$$

we obtain coefficient vectors for the basis functions $\mathcal{B}_{\mathcal{L}}$, and their gradients form a basis for $\mathcal{H}_{h,D,\mathrm{ex}}$. Once again, a similar procedure can be performed to obtain a basis for $\mathcal{H}_{h,N,\mathrm{co}}$.

Finally, once we have bases $\{Y_1,\dots,Y_{h^1}\}$ for $\mathcal{H}_{h,D}$ and $\{Z_1,\dots,Z_{m-1}\}$ for $\mathcal{H}_{h,D,\mathrm{ex}}$, a basis for $\mathcal{H}_{h,D,\partial\mathrm{co}}$ can be obtained e.g. by solving for the $2g$-dimensional kernel of the matrix

$$\left(\langle Z_i, Y_j\rangle_{L^2}\right)_{\substack{i=1,\dots,m-1\\ j=1,\dots,h^1}}$$

and orthonormalize with respect to $\mathcal{H}_{h,D,\mathrm{ex}}$, if necessary.

4.2. Computing discrete Hodge-type decompositions

Next, we present a computational approach for the decomposition of PCVFs according to the Hodge-type decomposition theorems derived in Section 3. The refined decompositions of discrete harmonic Dirichlet and Neumann fields provide a concise distinction between harmonic flows induced from the interior topological features of the geometry and those harmonic flows that reflect the boundary. We assume that we are given a PCVF $X \in \mathcal{X}_h$ which might come from real data or an analytic expression, and is L^2-projected onto the space $\mathcal{X}_h$, hence representing cell-averages of the original field, for instance.

To compute the decomposition, we follow the iterated L^2-projection approach proposed by Polthier and Preuss [8], since it is a conceptually simple and, due to its global nature, robust method: given a vector field $X = X_0 \in \mathcal{X}_h$, compute the L^2-projection $\mathrm{pr}_{\mathcal{V}_1}(X)$ onto an L^2-direct summand subspace $\mathcal{V}_1$ of the orthogonal decomposition of interest, and form the residue $X_1 := X - \mathrm{pr}_{\mathcal{V}_1}(X)$. Now, project X_1 onto the next subspace $\mathcal{V}_2$, form the residue X_2, and iterate until all subspaces are processed. Each projection step amounts to the solution of a linear problem of the type

$$\text{Find } u \in \mathcal{V}_i \text{ such that } \langle u, v\rangle_{L^2} = \langle X_{i-1}, v\rangle_{L^2} \quad \text{for all } v \in \mathcal{V}_i. \tag{19}$$

Solving these system requires a basis for each subspace $\mathcal{V}_i$ in order to set up the system matrix and the right-hand side. This is easy for the subspaces $\nabla\mathcal{L}_0$, $\nabla\mathcal{L}$, $J\nabla\mathcal{F}_0$ and $J\nabla\mathcal{F}$. Recall that for $\nabla\mathcal{L}$ and $J\nabla\mathcal{F}$, one should exclude the constant functions from the kernel, or solve for a least-squares minimum solution instead.

To compute the projection of X onto $\mathcal{H}_{h,D,\mathrm{ex}}$, we first compute a basis $\mathcal{B}_{\mathcal{H}_{h,D,\mathrm{ex}}} = \{Z_1,\dots,Z_{m-1}\}$ for $\mathcal{H}_{h,D,\mathrm{ex}}$ as described above. Each Z_i is of the form

$$Z_i = \sum_{j=1}^{n_V} z_{ij}\nabla\varphi_j \quad \text{with } \varphi_j \in \mathcal{L}$$

with coefficients $z_{ij} \in \mathbb{R}$. Using this basis, we now solve Eq. (19). The resulting coefficient vector u represents the solution as a linear combination

$$\sum_{i=1}^{m-1} u_i Z_i = \sum_{j=1}^{n_V}\left(\sum_{i=1}^{m-1} u_i z_{ij}\right)\nabla\varphi_j.$$

A pseudocode example for a computational decomposition according to Eq. (17) is given in 1. Of course, a computation for the decomposition involving the refined Neumann fields goes along the same lines.

Listing 1: Algorithm for the computation of the decomposition Eq. (17)

```
Input: PCVF X ∈ X_h, integer m (optional)
X_{∇L0}        = project(X, ∇L0)
X_1            = X - X_{∇L0}
X_{JF0}        = project(X_1, JF0)
X_2            = X_1 - X_{JF0}
X_{H∩JF}       = project(X_2, JF)
X_3            = X_2 - X_{H∩JF}
B_{H_{h,D,ex}} = compute_HDex_basis(size=m-1)
X_{H_{h,D,ex}} = project(X_3, B_{H_{h,D,ex}})
X_{H_{h,D,∂co}} = X_3 - X_{H_{h,D,ex}}
return X_{∇L0}, X_{JF0}, X_{H∩JF}, X_{H_{h,D,ex}}, X_{H_{h,D,∂co}}
```

Finally, we present two exemplary computational decompositions. The first one decomposes the L^2-projection to $\mathcal{X}_h$ of the vector field $X_{\mathrm{annulus}} = X_{N,\mathrm{co}} + X_{D,\mathrm{ex}} + X_{\mathrm{ex}} + X_{\mathrm{co}}$ with $X_{N,\mathrm{co}} = (x^2+y^2)^{-1}(-y,x)$, $X_{D,\mathrm{ex}} = (x^2+y^2)^{-1}(x,y)$, $X_{\mathrm{ex}} = (2x,1) = \nabla(x^2+y)$ and $X_{\mathrm{co}} = 2(-y,x) = -J\nabla(x^2+y^2)$ on a flat annulus in $\mathbb{R}^2$, centered at the origin. Since there is no inner cohomology (the annulus is homeomorphic to $\Sigma_{0,2}$), by Theorem 3.11 there is a complete L^2-orthogonal decomposition involving all the discussed spaces at the same time. Our result is shown in Fig. 7. The exact part X_{ex} contributes predominantly to the central harmonic space $\nabla\mathcal{L}\cap J\nabla\mathcal{F}$ and $\mathcal{H}_{h,D,\mathrm{ex}}$, whereas the harmonic circulation is correctly captured in $\mathcal{H}_{h,N,\mathrm{co}}$. The parts of the complete decomposition that are not shown correspond to the non-existing inner cohomology and are consequently negligible, with L^2-norms of order 10^{-12} and lower, see Table 1. Of course, a small discretization error depending on the mesh size stems from the projection step of the smooth field onto $\mathcal{X}_h$. The harmonic Dirichlet and Neumann components are in fact exact and coexact, respectively, as predicted by Lemma 3.10.

Our second example is a decomposition on a geometry of type $\Sigma_{5,4}$, see Fig. 8. The field to be decomposed is once again a superposition of several elementary fields: a harmonic circulation component around the right-most handle, a rotational global component and a divergence component in the center of the geometries. These fields are defined on the ambient space and projected to the triangles of M_h to obtain a discrete field $X_{\Sigma_{5,4}} \in \mathcal{X}_h$, which is then decomposed according to Eq. (16). As expected, we mainly find contributions in the subspaces $\nabla\mathcal{L}_0$, $J\nabla\mathcal{F}_0$ and $\mathcal{H}_{h,N,\partial\mathrm{co}}$, the latter reflecting the global harmonic flow around the "inner geometry" (the handles). See Table 1 for the L^2-norms for the components. The boundary behavior of all components in the decomposition is illustrated for one of the boundary holes in the close-up sequence in Fig. 9.

5. Conclusion and outlook

We presented a complete description for the structure of the space of piecewise constant vector fields on simplicial surfaces with boundary in terms of several Hodge-type decomposition theorems that are structurally consistent with the smooth theory. We used these results to compute refined decompositions for vector fields and bases for topologically significant subspaces of

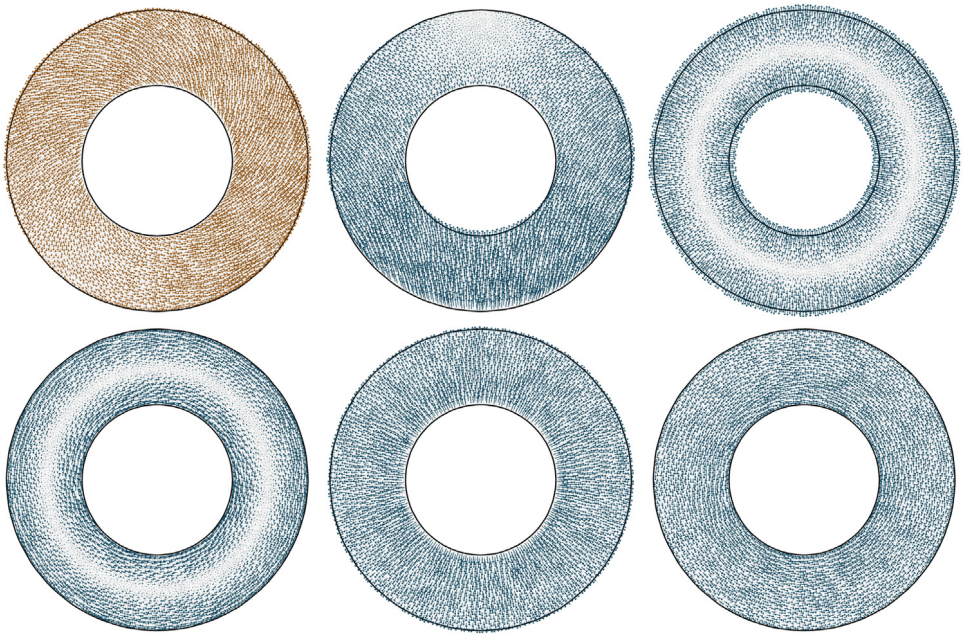

Fig. 7. Decomposition of the vector field X_{annulus}. Top row: input vector field, central harmonic component in $\nabla\mathcal{L} \cap J\nabla\mathcal{F}$ and exact component in $\nabla\mathcal{L}_0$. Bottom row: coexact component in $J\nabla\mathcal{F}_0$, exact Dirichlet component in $\mathcal{H}_{h,D,\text{ex}}$ and coexact Neumann component in $\mathcal{H}_{h,N,\text{co}}$. (For interpretation of the references to color in this figure legend, the reader is referred to the web version of this article.)

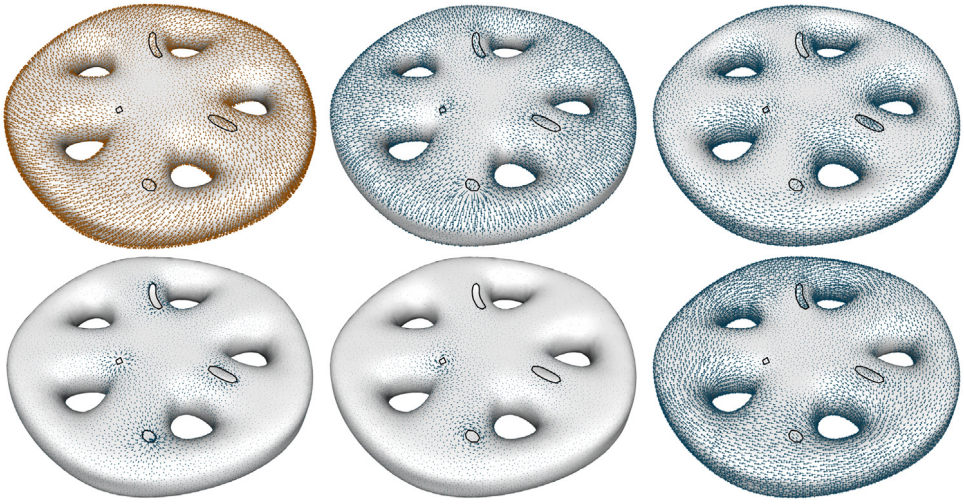

Fig. 8. Decomposition of the vector field $X_{\Sigma_{5,4}}$ on a surface of type $\Sigma_{5,4}$. Top row: input vector field, exact component in $\nabla\mathcal{L}_0$ and coexact component in $J\nabla\mathcal{F}_0$. Bottom row: harmonic exact component in $\mathcal{H}_h \cap \nabla\mathcal{L}$, coexact Neumann component in $\mathcal{H}_{h,N,\text{co}}$ and boundary-exact Neumann component in $\mathcal{H}_{h,N,\partial\text{ex}}$. (For interpretation of the references to color in this figure legend, the reader is referred to the web version of this article.)

Table 1
L^2-norms of the components of the decomposed vector fields. Entries with a hyphen do not exist in the computed decompositions.

Space	X_{annulus}	$X_{\Sigma_{5,4}}$	Space	X_{annulus}	$X_{\Sigma_{5,4}}$
Input	5.82	2.80			
$\nabla\mathcal{L}_0$	0.44	1.61	$\mathcal{H}_{h,D,\text{ex}}$	3.21	–
$\nabla\mathcal{F}_0$	0.89	1.08	$\mathcal{H}_{h,D,\partial\text{co}}$	10^{-12}	–
$\mathcal{H}_h \cap \nabla\mathcal{L}$	–	0.33	$\mathcal{H}_{h,N,\text{co}}$	4.33	0.06
$\nabla\mathcal{L} \cap J\nabla\mathcal{F}$	1.95	–	$\mathcal{H}_{h,N,\partial\text{ex}}$	10^{-14}	1.48

$\mathcal{X}_h$. Distinguishing between the inner and boundary cohomology representatives helps to identify intrinsic flows and flows that arise due to the presence of nontrivial boundary cycles individually. In addition, we found an obstruction not present in the smooth counterpart which needs to be considered for discretization strategies to obtain structurally consistent results, and we gave counterexamples to illustrate the problem.

We intend to build upon this work in various directions: since the validity of Eq. (12) is not only of theoretical interest, but crucial to obtain a consistent discretization, it is important to find a criterion that is easy to check computationally for a given simplicial surface M_h. On the computational side, we want to evaluate different solving strategies (e.g. a direct method based on a sparse QR decomposition) for the involved systems in terms of efficiency and robustness.

Acknowledgments

The authors thank the anonymous reviewers for their valuable feedback. The Laurent's hand model is provided courtesy of INRIA by the *AIM@SHAPE-VISIONAIR* Shape Repository. This work was

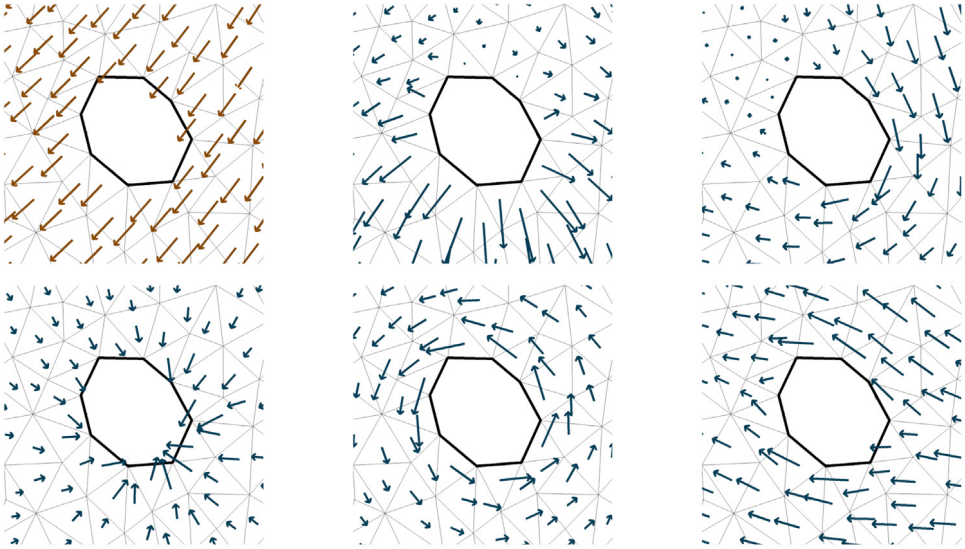

Fig. 9. Close-ups of the boundary behavior around the lower left boundary hole for the components from the decomposition in Fig. 8, following the same order as above. The exact component in $\nabla\mathcal{L}_0$ is perpendicular to the boundary (first row, second image), whereas the components of the harmonic Neumann part (second row, last two images) as well as the coexact component in $J\nabla\mathcal{F}_0$ (first row, last image) are mostly tangential, for they are L^2-orthogonal to all gradient fields, cf. Fig. 2. The harmonic exact component in $\mathcal{H}_h \cap \nabla\mathcal{L}$ does not obey any particular boundary behavior. Note that the backside of the surface is removed in this figure for better visibility. (For interpretation of the references to color in this figure legend, the reader is referred to the web version of this article.)

supported by the DFG Collaborative Research Center SFB/TRR 109 *Discretization in Geometry and Dynamics* and the *Berlin Mathematical School*.

References

[1] Schwarz G. Hodge decomposition: a method for solving boundary value problems. Lecture notes in mathematics, Springer; 1995.
[2] Shonkwiler C. Poincaré duality angles on Riemannian manifolds with boundary (Ph.D. thesis), University of Pennsylvania; 2009. thesis (Ph.D.).
[3] Shonkwiler C. Poincaré duality angles and the Dirichlet-to-Neumann operator. Inverse Problems 2013;29(4).
[4] Bhatia H, Norgard G, Pascucci V, Bremer P-T. The Helmholtz-Hodge decomposition—a survey. IEEE Trans Vis Comput Graphics 2013;19(8): 1386–404.
[5] Ahusborde E, Azaïez M, Caltagirone J-P, Gerritsma M, Lemoine A. Discrete Hodge—Helmholtz decomposition. Monogr Mat 2014;39:1–10.
[6] Bhatia H, Pascucci V, Bremer P-T. The natural Helmholtz-Hodge decomposition for open-boundary flow analysis. IEEE Trans Vis Comput Graphics 2014; 20(11):1566–78.
[7] Ribeiro PC, de Campos Velho HF, Lopes H. Helmholtz—Hodge decomposition and the analysis of 2D vector field ensembles. Comput Graph 2016.
[8] Polthier K, Preuss E. Identifying vector field singularities using a discrete Hodge decomposition. In: Hege H-C, Polthier K, editors. Visualization and mathematics III. Springer Verlag; 2003. p. 113–34.
[9] Wardetzky M. Discrete differential operators on polyhedral surfaces—convergence and approximation (Ph.D. thesis), Berlin: Freie Universität Berlin; 2006.
[10] Hirani AN. Discrete exterior calculus (Ph.D. thesis), Pasadena, (CA), (USA). 2003.
[11] Hirani AN, Kalyanaraman K, Wang H, Watts S. Cohomologous harmonic cochains. Available as e-print on arxiv.org, 2011. URL: http://arxiv.org/abs/1012.2835.
[12] Arnold DN, Falk RS, Winther R. Finite element exterior calculus, homological techniques, and applications. Acta Numer 2006;15:1–155.
[13] Holst M, Stern A. Geometric variational crimes: Hilbert complexes, finite element exterior calculus, and problems on hypersurfaces. Found Comput Math 2012;12(3):263–93.
[14] Bochev PB, Hyman JM. Principles of mimetic discretizations of differential operators. In: Arnold DN, Bochev PB, Lehoucq RB, Nicolaides RA, Shashkov M, editors. Compatible spatial discretizations. The IMA volumes in mathematics and its applications, vol. 142. New York: Springer; 2006.
[15] Lipnikov K, Manzini G, Brezzi F, Buffa A. The mimetic finite difference method for the 3D magnetostatic field problems on polyhedral meshes. J Comput Phys 2011;230(2):305–28.
[16] Xu K, Zhang H, Cohen-Or D, Xiong Y. Dynamic harmonic fields for surface processing. Comput Graph 2009;33(3):391–8. {IEEE} International Conference on Shape Modelling and Applications 2009.
[17] Schall O, Zayer R, Seidel H. Controlled field generation for quad-remeshing. In: Proceedings of the 2008 ACM symposium on solid and physical modeling, Stony Brook, New York, USA, June 2–4, 2008, 2008, pp. 295–300.
[18] Tong Y, Alliez P, Cohen-Steiner D, Desbrun M. Designing quadrangulations with discrete harmonic forms. In: Proceedings of the fourth eurographics symposium on geometry processing. SGP '06, Eurographics Association; 2006. p. 201–10.
[19] Dong S, Kircher S, Garland M. Harmonic functions for quadrilateral remeshing of arbitrary manifolds. Comput Aided Geom Design 2005;22(5):392–423.
[20] Abraham R, Marsden J, Ratiu T. Manifolds, tensor analysis, and applications. 2nd ed. Springer; 1988.
[21] Friedrichs KO. Differential forms on Riemannian manifolds. Comm Pure Appl Math 1955;8(4):551–90.
[22] Marsden J, Hoffman M. Basic complex analysis. W. H. Freeman; 1999.
[23] Whitney H. Geometric integration theory. Princeton legacy library, Princeton University Press; 1957.
[24] Alnæs M, Blechta J, Hake J, Johansson A, Kehlet B, Logg A, et al. The FEniCS project version 1.5. Arch Numer Softw 2015;3(100).
[25] Logg A, Mardal K-A, Wells GN, editors. Automated solution of differential equations by the finite element method. Lecture notes in computational science and engineering, vol. 84. Springer; 2012.
[26] Polthier K, Khadem S, Preuss E, Reitebuch U. Publication of interactive visualizations with JavaView. In: Borwein J, Morales M, Rodrigues J, Polthier K, editors. Multimedia tools for communicating mathematics. Mathematics and visualization, Berlin, (Heidelberg): Springer; 2002. p. 241–64. URL: www.javaview.de.
[27] Lehoucq R, Sorensen D, Yang C. ARPACK users' guide. Society for Industrial and Applied Mathematics; 1998.
[28] Pinkall U, Polthier K. Computing discrete minimal surfaces and their conjugates. Experiment Math 1993;2(1):15–36.
[29] Rognes ME, Ham DA, Cotter CJ, McRae ATT. Automating the solution of PDEs on the sphere and other manifolds in FEniCS 1.2. Geosci Model Dev 2013;6(6): 2099–119.
[30] Erickson J, Whittlesey K. Greedy optimal homotopy and homology generators. In: Proceedings of the sixteenth annual ACM–SIAM symposium on discrete algorithms. SODA '05, Society for Industrial and Applied Mathematics; 2005. p. 1038–46.
[31] Dłotko P. A fast algorithm to compute cohomology group generators of orientable 2-manifolds. Pattern Recognit Lett 2012;33(11):1468–76. computational Topology in Image Context.
[32] Busaryev O, Cabello S, Chen C, Dey TK, Wang Y. Annotating simplices with a homology basis and its applications. In: Algorithm theory—SWAT 2012: 13th scandinavian symposium and workshops, Helsinki, Finland, July 4–6, 2012. Proceedings. Berlin, Heidelberg: Springer; 2012. p. 189–200.